

Energy-momentum tensor form factor $D(t)$ of proton and neutron

Andrea Mejia and Peter Schweitzer

Department of Physics, University of Connecticut, Storrs, CT 06269-3046, U.S.A.

(Dated: November 2025)

The energy-momentum tensor (EMT) form factor $D(t)$ is finite and negative in hadronic models and lattice QCD when only strong forces are included. However, when electromagnetic forces are considered, the $D(t)$ of charged hadrons undergoes a dramatic change: at small t , it changes sign and diverges like $1/\sqrt{-t}$ as shown for the proton in the classical model by Białynicki-Birula based on residual nuclear forces which can be understood as a mean field approach. We construct an analogous neutron model and show that this framework accurately explains the electromagnetic proton-neutron mass difference. We demonstrate that, after appropriately rescaling the residual nuclear forces, the model can reproduce lattice data on the nucleon $D(t)$ up to $(-t) \lesssim 1 \text{ GeV}^2$ as well as QED effects. Based on this realistic model description, we show that the proton and neutron $D(t)$ form factors are practically indistinguishable down to $(-t) \approx 10^{-4} \text{ GeV}^2$ far below what can currently be accessed experimentally. We conclude that in the foreseeable future the $D(t)$ form factors of proton and neutron will practically look the same in experiments and phenomenology.

PACS numbers: 03.50.-z, 11.27.+d, 14.20.Dh

Keywords: energy momentum tensor, composed particle, classical models, D -term, QED effects

I. INTRODUCTION

Hadronic EMT form factors [1, 2] can be accessed via generalized parton distribution functions in hard exclusive reactions [3, 4] and contain key information about the structure of hadrons. This work is focused on the EMT form factor $D(t)$ also known as the D -term form factor [5] which has an appealing interpretation in terms of forces inside hadrons [6–8], see the reviews [9–11]. In closed systems governed by strong (short-range) forces, $D(t)$ is negative and finite [12–38]. But when electromagnetic (long-range) forces are included then, at small t , $D(t)$ changes sign and diverges like $1/\sqrt{-t}$ as shown for charged pions in chiral perturbation theory [39] and for proton in a classical model [40]. This divergence is a universal QED effect specific to all charged particles [41–43] that emerges also for non-hadronic systems [44] and for other types of long-range forces [45]. The neutron of course does not exhibit such a divergence which gives rise to important practical questions. Can the divergence of the proton $D(t)$ be seen experimentally? Must the proton and neutron be treated differently in phenomenological studies of hard exclusive reactions?

The purpose of this work is to address such questions. For that we will, after introducing the notation and EMT form factors (Sec. II), review the model by Białynicki-Birula (Sec. III) [46] explored in the aforementioned study of the proton $D(t)$ [40]. We construct an analogous neutron model (Sec. IV). Among other results, an interesting highlight is that this simple framework provides an accurate description of the electromagnetic proton-neutron mass difference (Sec. V). Equipped with this framework, we investigate the neutron EMT properties and compare to proton results [40] (Sec. VI) demonstrating the usefulness of the concept of a “regularized” proton D -term proposed in [40]. We discuss how to define the neutron size which, unlike the proton case, cannot be associated with the mean square charge radius — but can be well defined in terms of EMT radii (Sec. VII). The residual nuclear forces are not strong enough to yield a $D(t)$ as large as seen in hadronic models or lattice QCD, but we will show that they can be scaled up to reproduce lattice QCD data on $D(t)$ of nucleon up to $(-t) \lesssim 1 \text{ GeV}^2$ (Sec. VIII). Based on this realistic description of $D(t)$ of proton and neutron, which is consistent with QED and QCD predictions, we show that the $D(t)$ of proton and neutron can be expected to be practically indistinguishable and QED effects become noticeable in the proton $D(t)$ only at very small $(-t) \lesssim 10^{-5} \text{ GeV}^2$. Finally, we present our conclusions (Sec. IX).

In this work we will indirectly (in a “reversed mode”) make use of the interpretation of $D(t)$ and other form factors in terms of 3D spatial densities [6] which met also criticism, see the review [11] and references therein. However, the main points of criticism do not apply to this work. For instance, the classical model used in this work can be understood as a mean field approach to the description of the nucleon, a well justified concept in the large- N_c limit in QCD [50]. In this limit, the nucleon mass grows as $M \propto N_c$ making relativistic recoil corrections negligible [9–11]. In such a situation, the criticism of exploring the Breit frame for the interpretation of form factors as 3D densities [47] does not apply, because the motion of the nucleon as a whole is non-relativistic — while that of its constituents can be highly relativistic [34]. Other criticism related to the notion of pressure in quantum systems [48] also does not directly apply to our approach because in classical frameworks concepts like pressure are unambiguously defined to begin with. For a more complete overview of this aspect, we refer to [11] and [47–49] for the latest developments.

II. EMT FORM FACTORS AND SPATIAL DISTRIBUTIONS

The nucleon form factors of the total symmetric EMT operator $\hat{T}^{\mu\nu}$ are defined as follows [1, 2]

$$\langle p' | \hat{T}^{\mu\nu} | p \rangle = \bar{u}(p') \left[A(t) \frac{P^\mu \gamma^\nu + P^\nu \gamma^\mu}{2} + B(t) \frac{i(P^\mu \sigma^{\nu\rho} + P^\nu \sigma^{\mu\rho}) \Delta_\rho}{4M} + D(t) \frac{\Delta^\mu \Delta^\nu - g^{\mu\nu} \Delta^2}{4M} \right] u(p) \quad (1)$$

where $P = \frac{1}{2}(p' + p)$, $\Delta = p' - p$, $t = \Delta^2$. The spinors are normalized as $\bar{u}(p) u(p) = 2M$ with spin indices omitted for brevity. In the Breit frame where $p^\mu = (E, -\frac{1}{2}\vec{\Delta})$, $p'^\mu = (E, \frac{1}{2}\vec{\Delta})$ and $t = -\vec{\Delta}^2$, the static EMT tensor is defined as

$$T^{\mu\nu}(\vec{r}) = \int \frac{d^3\Delta}{2E(2\pi)^3} \langle p', s' | \hat{T}^{\mu\nu} | p, s \rangle e^{-i\vec{\Delta} \cdot \vec{r}}. \quad (2)$$

Here $T_{00}(\vec{r})$ denotes the energy density that yields the particle mass as $M = \int d^3r T_{00}(\vec{r})$ and is given by [9]

$$T_{00}(r) = M \int \frac{d^3\Delta}{(2\pi)^3} e^{-i\vec{\Delta} \cdot \vec{r}} \left(A(t) + \frac{t}{4m^2} (B(t) - D(t)) \right) \quad (3)$$

$T_{0k}(\vec{r})$ is related to the angular momentum distribution. The spatial components describe the stress tensor

$$T^{ij}(\vec{r}) = \left(\frac{r^i r^j}{r^2} - \frac{\delta^{ij}}{3} \right) s(r) + \delta^{ij} p(r) \quad (4)$$

where $s(r)$ is the shear force and $p(r)$ the pressure in the system [9] which can be determined from $D(t)$ as follows

$$s(r) = -\frac{1}{4M} r \frac{d}{dr} \left[\frac{1}{r} \frac{d}{dr} \tilde{D}(r) \right], \quad p(r) = \frac{1}{6M} \frac{1}{r^2} \frac{d}{dr} \left[r^2 \frac{d}{dr} \tilde{D}(r) \right], \quad \tilde{D}(r) = \int \frac{d^3\Delta}{(2\pi)^3} e^{-i\vec{\Delta} \cdot \vec{r}} D(-\vec{\Delta}^2). \quad (5)$$

Due to EMT conservation, $\nabla^i T^{ij}(\vec{r}) = 0$ which implies the following differential relation and the von Laue condition

$$(a) \quad \frac{2}{3} s'(r) + \frac{2}{r} s(r) + p'(r) = 0, \quad (b) \quad \int_0^\infty dr r^2 p(r) = 0. \quad (6)$$

Mechanical stability imposes on the normal force (per unit area) $\frac{2}{3}s(r) + p(r)$ the condition [24]

$$\frac{2}{3} s(r) + p(r) \geq 0, \quad (7)$$

which holds in systems with short range forces [11]. The D -term $D = D(0)$ can be computed in two equivalent ways

$$D = D_{\text{press}} = D_{\text{shear}}, \quad D_{\text{press}} = M \int d^3r r^2 p(r), \quad D_{\text{shear}} = -\frac{4}{15} M \int d^3r r^2 s(r). \quad (8)$$

Two interesting quantities are the mechanical and mass mean square radii defined as

$$\langle r_{\text{mech}}^2 \rangle = \frac{\int d^3r r^2 \left(\frac{2}{3} s(r) + p(r) \right)}{\int d^3r \left(\frac{2}{3} s(r) + p(r) \right)} = \frac{6D}{\int_{-\infty}^0 dt D(t)}, \quad \langle r_{\text{mass}}^2 \rangle = \frac{\int d^3r r^2 T_{00}(r)}{\int d^3r T_{00}(r)} = 6A'(0) - \frac{3D}{2M^2}. \quad (9)$$

It is important to point out, that in classical frameworks one deals with a “reversed” situation in the following sense. Form factors are the primary properties in nature that can be determined experimentally or computed in quantum field theoretical models, lattice QCD or other approaches. The 3D spatial distributions are secondary properties based on interpretations [9–11]. In classical models, the situation is opposite. Here the 3D spatial distributions are the primary properties that can be directly computed, and the evaluation of form factors in classical frameworks is based on inverting the Fourier transforms in Eqs. (3, 5). One could, of course, wonder whether classical frameworks can be applied to describe particles. However, the model description of the proton “is not out of touch with reality” [46] and, as noted in Sec. I, this fully relativistic field theoretical framework can be viewed as a simple model of a quantum mean field approach which allays any doubts.

The interpretation of form factors in terms of 3D distributions is justified when the hadron size R is much larger than its Compton wavelength λ_C . For instance, this condition is well justified for nuclei, not at all for pions, and the nucleon is a border case as assessed in [29]. In the nucleon case, however, the interpretation becomes exact in the limit of a large number of colors N_c where baryons can be described in the mean field approach as classical solitons of mesonic fields [50] and the nucleon mass grows as $M \propto N_c$ making relativistic recoil corrections negligible [9–11]. In classical models, the starting point are exactly known 3D spatial distributions, and the inversion of the Fourier transforms in Eqs. (3, 5) yields reliable results for $(-t) \lesssim 1 \text{ GeV}^2$ [51–53]. We will make a similar observation regarding the range of applicability for EMT form factor computations in the present approach.

III. CLASSICAL PROTON MODEL

In the classical model [46], the proton is made of dust of total mass m_{dust} which is bound within a spherical region of radius R by the interplay of three forces — attractive strong force mediated by the scalar field ϕ with mass m_s , repulsive strong force mediated by the vector field V^μ with mass m_v , and electromagnetic force described by the four-potential A^μ — to which the dust particles couple through the pertinent coupling constants g_s , g_v , e . The dynamics of the system is described by covariant field equations which can be found in Ref. [46] and are most conveniently solved in the rest frame of the system where the fields are time-independent, A^α and V^α have no spatial components, and the dust is described by a static distribution $\rho(r)$. In this frame, the classical field equations are given by [46]

$$\rho \vec{\nabla} (g_v V_0 + e A_0 - g_s \phi) = 0, \quad (10a)$$

$$(-\Delta + m_v^2) V_0 = g_v \rho, \quad (10b)$$

$$(-\Delta + m_s^2) \phi = g_s \rho, \quad (10c)$$

$$-\Delta A_0 = e \rho. \quad (10d)$$

The dust density is normalized as $\int d^3r \rho(r) = 1$. The solutions of Eqs. (10) are given by [46] (we use “ p ” and “ n ” to label model quantities and “prot” and “neut” to label physical quantities of proton and neutron)

$$\rho_p(r) = \left(f_p^+(r) - f_p^-(r) \right) \Theta(R_p - r), \quad (11a)$$

$$e A_p^0(r) = e^2 \left(\frac{f_p^+(r)}{(k_p^+)^2} - \frac{f_p^-(r)}{(k_p^-)^2} + \frac{2E_B^p}{e^2} \right) \Theta(R_p - r) + \frac{e^2}{4\pi r} \Theta(r - R_p), \quad (11b)$$

$$g_s \phi_p(r) = g_s^2 \left(\frac{f_p^+(r)}{(k_p^+)^2 + m_s^2} - \frac{f_p^-(r)}{(k_p^-)^2 + m_s^2} \right) \Theta(R_p - r) + \frac{b_s^p}{4\pi r} e^{-m_s(r-R_p)} \Theta(r - R_p), \quad (11c)$$

$$g_v V_p^0(r) = g_v^2 \left(\frac{f_p^+(r)}{(k_p^+)^2 + m_v^2} - \frac{f_p^-(r)}{(k_p^-)^2 + m_v^2} \right) \Theta(R_p - r) + \frac{b_v^p}{4\pi r} e^{-m_v(r-R_p)} \Theta(r - R_p), \quad (11d)$$

with (a misprint in the definition of k_p^\pm in Eq. (23) of [46] was fixed in Eq. (15) of [40])

$$f_p^\pm(r) = \frac{d_p^\pm \sin(k_p^\pm r)}{4\pi r}, \quad k_p^\pm = \sqrt{\frac{B_p \pm \sqrt{C_p}}{2Q_p^2}},$$

$$B_p = (g_s^2 - e^2)m_v^2 - (g_v^2 + e^2)m_s^2, \quad C_p = B_p^2 - 4e^2Q_p^2m_s^2m_v^2, \quad Q_p = \sqrt{g_v^2 + e^2 - g_s^2}. \quad (11e)$$

The six constants b_v^p , b_s^p , d_+^p , d_-^p , E_B^p , R_p can be fixed from the continuity and differentiability conditions of the fields $A_p^0(r)$, $V_p^0(r)$, $\phi_p(r)$ at $r = R_p$, and the normalization condition $\int d^3r \rho_p(r) = 1$ can be used as a cross check. Restoring here \hbar and c for convenience, the proton model parameters are given by [46]

$$m_s c^2 = 550 \text{ MeV}, \quad m_v c^2 = 783 \text{ MeV}, \quad \frac{g_s^2}{\hbar c} = 91.64, \quad \frac{g_v^2}{\hbar c} = 136.2, \quad \alpha = \frac{e^2}{4\pi\hbar c} = \frac{1}{137}, \quad (12)$$

The scalar and vector fields correspond to σ - and ω -mesons with the values of m_s , m_v , g_s , g_v taken from the QHD-I mean field theory model of nuclear matter [54]. For these parameters, it follows $b_v^p = 1354.13 \text{ MeV fm}$, $b_s^p = 1786.38 \text{ MeV fm}$, $d_+^p = 2.02477/\text{fm}^2$, $d_-^p = -3.93639/\text{fm}^2$, $E_B^p = -15.7089 \text{ MeV}$, $R_p = 1.04906 \text{ fm}$ from the boundary conditions of the fields at $r = R_p$. We set $m_{\text{dust}} = 953.981 \text{ MeV}$.¹

The proton mass is $M_{\text{prot}} = m_{\text{dust}} + E_B^p$ where the binding energy $E_B^p = -15.71 \text{ MeV}$ [46] is to be compared to the bulk binding energy per nucleon in nuclear matter of -15.75 MeV [54]. Since the dust in the proton model is bound by same nuclear forces that bind nuclei in nuclear matter, this is an important consistency check of the model [46]. The mean square dust radius given by $\langle r_{\text{dust}}^2 \rangle = \int d^3r r^2 \rho(r)$ yields the proton charge radius whose numerical value 0.710 fm in the model underestimates the experimental result by 15 % but is “not completely out of touch with reality” [46] making this model sufficient for the purposes of Refs. [40, 46] (and this work until Sec. VIII).

¹ In Refs. [40, 46] m_{dust} was set equal to the physical proton mass with the model result for the proton mass corresponding to the mass of a proton bound in infinite nuclear matter [46]. Throughout this work, we choose a different scheme and identify m_{dust} with a “bare proton mass” such that, after including the binding energy, the sum $m_{\text{dust}} + E_B^p$ reproduces the physical value of the proton mass of 938.272 MeV [57]. This is the only difference regarding parameter fixing between Refs. [40, 46] and this work until Sec. VIII.

IV. CLASSICAL NEUTRON MODEL

We proceed with the construction of the analogous neutron model by keeping everything exactly as in the proton case, except for “removing” the electromagnetic interaction. In this way, the only difference between proton and neutron is due to electromagnetic effects. We make no effort to attempt considering isospin breaking effects.

Notice that by taking the limit $e \rightarrow 0$ in Eqs. (10) the dust becomes electrically neutral. This implies that the neutron electric form factor $G_{En}(t)$ vanishes. Experimentally, $G_{En}(t)$ is found much smaller than the proton electric form factor $G_{Ep}(t)$. Numerically, $G_{En}(t)/G_{Ep}(t) \lesssim 20\%$ in the region $0 \leq (-t) \lesssim 1 \text{ GeV}^2$ [55] (which, as we shall see, corresponds to the range of applicability of this approach). To the extent that this number can be considered numerically small, one may argue that we neglect a small effect. More importantly, with the main focus of this work on mechanical (rather than electrical) properties, this simple neutron model is sufficient.

In the limit $e \rightarrow 0$, the Poisson equation (10d) becomes a Laplace equation with the simple solution $A_0(r) = 0$. The static field equations (10a-d) are replaced in the neutron case by

$$\rho \vec{\nabla}(g_v V_0 - g_s \phi) = 0, \quad (13a)$$

$$(-\Delta + m_v^2)V_0 = g_v \rho, \quad (13b)$$

$$(-\Delta + m_s^2)\phi = g_s \rho \quad (13c)$$

with $\int d^3r \rho(r) = 1$ and $\rho(r) = 0$ for $r > R_n$ as in the proton case. The solution of (13) can be derived from the proton solution (11) by taking the limit $e \rightarrow 0$. In this limit

$$\lim_{e \rightarrow 0} B_p = \lim_{e \rightarrow 0} \sqrt{C_p} = g_s^2 m_v^2 - g_v^2 m_s^2 \equiv B_n, \quad \lim_{e \rightarrow 0} Q_p = \sqrt{g_v^2 - g_s^2} \equiv Q_n. \quad (14a)$$

For $e \rightarrow 0$ the constant k_p^+ has a finite limit, but k_p^- vanishes according to

$$\lim_{e \rightarrow 0} k_p^+ = k_n^+ = \frac{\sqrt{B_n}}{Q_n}, \quad k_p^- = e \frac{m_s m_v}{\sqrt{B_n}} + \mathcal{O}(e^2) \rightarrow 0. \quad (14b)$$

The latter implies that in Eq. (11b) the limit $e \rightarrow 0$ must be taken with care. This equation yields the constraint

$$\lim_{e \rightarrow 0} e A_p^0(r) = \lim_{e \rightarrow 0} \left(2E_B^p - \frac{e^2 f_p^-(r)}{(k_p^-)^2} \right) = 2E_B^n - \frac{\sqrt{B_n}}{m_s m_v} \lim_{e \rightarrow 0} \frac{e d_-^p}{4\pi} \stackrel{!}{=} 0. \quad (14c)$$

Since the dust in the neutron must be bound, we expect $E_B^n \neq 0$. This implies that in Eq. (14c) the constant d_-^p must diverge as $1/e$. The divergent constant d_-^p appears always inside $f_p^-(r)$ in combination with $\sin(k_p^- r)$. In this combination the divergence of $d_-^p \propto 1/e$ and the vanishing of $k_p^- \propto e$ compensate each other such that

$$\lim_{e \rightarrow 0} f_p^-(r) = \lim_{e \rightarrow 0} \frac{d_-^p \sin(k_p^- r)}{4\pi r} = \lim_{e \rightarrow 0} \frac{d_-^p k_p^-}{4\pi} = \frac{2m_s^2 m_v^2}{B_n} E_B^n \equiv f_n^-(r). \quad (14d)$$

In other words, in the neutron case the function $f_n^-(r)$ becomes a constant, while $f_n^+(r)$ retains the same form as in the proton case, albeit with different constants.

Summarizing these findings in a notation chosen to maximally resemble the notation of the proton solutions (11), we obtain the neutron solutions (labeled by “n” for the neutron) given by

$$\rho_n(r) = \left(f_+^n(r) - f_-^n(r) \right) \Theta(R_n - r), \quad (15a)$$

$$g_s \phi_n(r) = g_s^2 \left(\frac{f_+^n(r)}{(k_n^+)^2 + m_s^2} - \frac{f_-^n(r)}{(k_n^-)^2 + m_s^2} \right) \Theta(R_n - r) + \frac{b_s^n}{4\pi r} e^{-m_s(r-R_n)} \Theta(r - R_n), \quad (15b)$$

$$g_v V_0^n(r) = g_v^2 \left(\frac{f_+^n(r)}{(k_n^+)^2 + m_v^2} - \frac{f_-^n(r)}{(k_n^-)^2 + m_v^2} \right) \Theta(R_n - r) + \frac{b_v^n}{4\pi r} e^{-m_v(r-R_n)} \Theta(r - R_n), \quad (15c)$$

with the functions $f_n^\pm(r)$ and constants k_n^\pm given by

$$f_+^n(r) = \frac{d_+^n \sin(k_n^+ r)}{4\pi r}, \quad f_-^n(r) = \frac{2m_s^2 m_v^2}{B_n^2} E_B^n, \quad k_n^+ = \frac{\sqrt{B_n}}{Q_n}, \quad (15d)$$

$$B_n = g_s^2 m_v^2 - g_v^2 m_s^2, \quad Q_n = \sqrt{g_v^2 - g_s^2}.$$

The five constants b_v^n , b_s^n , d_+^n , E_B^n , R_n are fixed by the continuity and differentiability conditions of the scalar and vector fields at $r = R_n$ and the normalization $\int d^3r \rho_n(r) = 1$. With the choice of parameters as in the proton case in Eq. (12) (except that e is set to zero) the constants assume the values $b_v^n = 1381.63 \text{ MeV fm}$, $b_s^n = 1816.96 \text{ MeV fm}$, $d_+^n = 2.06438 \text{ fm}^2$, $E_B^n = -16.6614 \text{ MeV}$, $R_n = 1.03958 \text{ fm}$. We discuss the results of this model in the next section.

V. NEUTRON AND PROTON EMT DISTRIBUTIONS

In Fig. 1 we show the neutron results in comparison to the proton results from Ref. [40] for the dust distribution $\rho(r)$ and the potentials multiplied by the respective coupling constants, $g_s\phi(r)$, $g_v V_0(r)$, $eA_0(r)$. Notice that $R_n = 1.04$ fm vs $R_p = 1.05$ fm which implies that the neutron is slightly smaller than the proton (we will discuss the question how to define the neutron size in detail in Sec. VII). We observe in Fig. 1 that $\rho(r)$, $g_s\phi(r)$, $g_v V_0(r)$ of the neutron are slightly larger in the inner region up to $r \lesssim 0.9$ fm than the corresponding proton functions. Around $r \approx 0.9$ fm the picture flips and the proton functions are slightly larger as illustrated by the inserts in Figs. 1a-c. The Coulomb potential is much smaller than the strong fields in the proton and identically zero in the neutron — which makes the difference. The electrostatic repulsion of the charged dust leads to a “swelling” of the proton as compared to the neutron. The dust distribution is therefore more compact in the neutron. Since the dust is also the source of the strong fields, the latter are slightly more strongly localized in the neutron.

Next we discuss the EMT densities $T_{00}(r)$, $p(r)$, $s(r)$ whose model expressions are given by [40, 46]

$$T_{00}(r) = T_{00}(r)_{\text{strong}} + T_{00}(r)_{\text{em}}, \quad p(r) = p(r)_{\text{strong}} + p(r)_{\text{em}}, \quad s(r) = s(r)_{\text{strong}} + s(r)_{\text{em}}, \quad (16a)$$

where

$$T_{00}(r)_{\text{strong}} = +\frac{1}{2}\phi'(r)^2 + \frac{1}{2}V_0'(r)^2 + \frac{1}{2}m_s^2\phi(r)^2 + \frac{1}{2}m_v^2V_0(r)^2 + (m_{\text{dust}} - g_s\phi(r))\rho(r), \quad (16b)$$

$$p(r)_{\text{strong}} = -\frac{1}{6}\phi'(r)^2 + \frac{1}{6}V_0'(r)^2 - \frac{1}{2}m_s^2\phi(r)^2 + \frac{1}{2}m_v^2V_0(r)^2, \quad (16c)$$

$$s(r)_{\text{strong}} = \phi'(r)^2 - V_0'(r)^2, \quad (16d)$$

$$T_{00}(r)_{\text{em}} = \frac{1}{2}A_0'(r)^2, \quad (16e)$$

$$p(r)_{\text{em}} = \frac{1}{6}A_0'(r)^2, \quad (16f)$$

$$s(r)_{\text{em}} = -A_0'(r)^2, \quad (16g)$$

with the understanding that these expressions are to be evaluated with respectively $\rho_p(r)$, $\phi_p(r)$, $V_p^0(r)$, $A_p^0(r)$ in Eqs. (11a-f) in the proton case, and with $\rho_n(r)$, $\phi_n(r)$, $V_n^0(r)$ in Eqs. (15a-e) and the Coulomb potential set to zero in the neutron case. In Figs. 2a-d we show the EMT distributions as functions of r for neutron in comparison to the proton results [40]. In the region $r \lesssim 2$ fm, the proton and neutron distributions look much alike up to about 1 fm. The neutron exhibits a slightly larger energy density and slightly stronger forces, appearing more compact compared to the slightly more spread out proton. These effects are small because in the inner region where the dust is located, the Coulomb force is overwhelmed by the strong forces.

The picture is crucially different in the outer region $r \gtrsim 2$ fm illustrated by the inserts in Figs. 2a-d. Here, the neutron distributions exhibit exponential decays governed by the Yukawa tail of the scalar field (the more massive vector field decays faster) while the proton densities exhibit power decays dictated by the Coulomb field, see Table I. Overall, in the neutron: (i) $s(r)$ is always positive, (ii) $p(r)$ remains negative after exhibiting a single node, (iii) $\frac{2}{3}s(r) + p(r)$ is always positive. These are common features found for ground state solutions of systems governed by short-range forces [9]. These features are also observed in the proton up to distances $r \lesssim 2$ fm. Beyond that point,

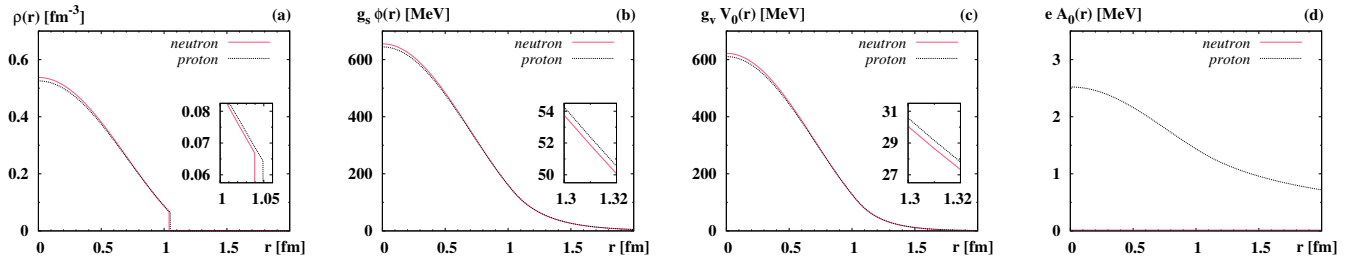


FIG. 1: Dust distribution $\rho(r)$, scalar potential $g_s\phi(r)$, vector potential $g_v V_0(r)$, and Coulomb potential $eA_0(r)$ as functions of r in the neutron (this work) and proton [40]. The inserts illustrate that the fields are more strongly localized in the neutron.

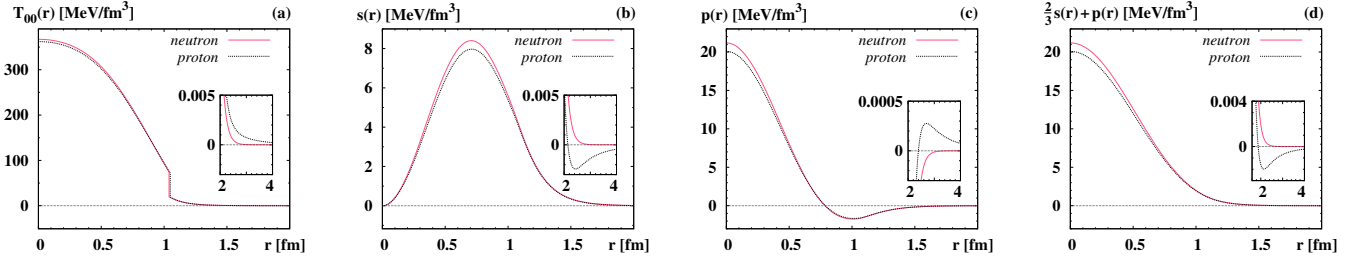


FIG. 2: EMT densities $T_{00}(r)$, $s(r)$, $p(r)$ and normal force per unit area $\frac{2}{3}s(r) + p(r)$ as functions of r for neutron (this work) and proton [40]. The inserts show the outer regions $r \gtrsim 2$ fm where the QED effects are manifest.

however, the Coulomb contribution begins to dominate the proton asymptotics, and: (i) causes $s(r)$ to turn negative (insert of Fig. 2b), (ii) generates a second node in $p(r)$ turning it positive at large r (insert of Fig. 2c), (iii) makes $\frac{2}{3}s(r) + p(r)$ become negative (insert of Fig. 2d). In short, the effect of the long-range Coulomb field is to reverse signs of $s(r)$, $p(r)$ and the normal force as observed in [40]. This large-distance behavior of the EMT distributions is a generic QED effect arising from one-loop QED corrections [40–43].

To demonstrate the theoretical consistency of the approach, let us mention that the differential equation (6a) holds in the neutron and proton models, and forces in the von Laue condition (6b) balance each other exactly as follows

$$\begin{aligned} \text{neutron: } \int_0^\infty dr r^2 p_i(r) &= \begin{cases} -11.092 \text{ MeV} & \text{for } i = \text{scalar}, \\ 11.092 \text{ MeV} & \text{for } i = \text{vector}, \end{cases} \\ \text{proton: } \int_0^\infty dr r^2 p_i(r) &= \begin{cases} -10.916 \text{ MeV} & \text{for } i = \text{scalar}, \\ 10.891 \text{ MeV} & \text{for } i = \text{vector}, \\ 0.025 \text{ MeV} & \text{for } i = \text{Coulomb}, \end{cases} \end{aligned} \quad (17)$$

which reinforces what we saw in Fig. 2: in the neutron the forces are slightly larger than in the proton. In the neutron, the normal forces (7) are always positive. In the proton, they are positive up 1.88 fm, see Fig. 2d and Table I. As there is no dust at that distance, the latter this does not impact the mechanical stability of the proton [40].

Finally, we discuss the proton-neutron mass difference. We remind that in this model isospin violating effects are not considered and the proton-neutron mass difference is entirely due to electromagnetic effects. We obtain a very good agreement with a lattice QCD study where QED effects were considered [56]

$$\begin{aligned} \text{classical model: } (M_{\text{prot}} - M_{\text{neut}})_{\text{e.m.}} &= (E_B^p - E_B^n) = 0.95 \text{ MeV}, \\ \text{lattice QCD+QED: } (M_{\text{prot}} - M_{\text{neut}})_{\text{e.m.}} &= (1.00 \pm 0.07_{\text{stat}} \pm 0.14_{\text{syst}}) \text{ MeV}, \end{aligned} \quad (18)$$

The fact that electromagnetic effects make the proton mass larger compared to the neutron mass can also be intuitively understood in the classical model. One can think of “assembling” the proton solution from a neutron solution by moving electric charges from infinity to a finite volume within the radius R_p which requires a work $W_{\text{el}} = (M_p - M_n)_{\text{e.m.}} = 0.95 \text{ MeV}$ to overcome the electrostatic repulsion which includes a slight rearrangement of the dust distribution (this “thought experiment” assumes that the dust particles can carry any continuous amount of electric charge and there is no confinement which is the case [46] in the model). In nature, isospin breaking effects due to the current quark masses $m_d > m_u$ make a contribution that is larger and of opposite sign to Eq. (18) [56] which explains the experimental observation $(M_n - M_p)_{\text{exp}} = 1.293 \text{ MeV}$ [57].

	$T_{00}(r)$	$s(r)$	$p(r)$	$\frac{2}{3}s(r) + p(r)$
neutron	$c_n \frac{m_s^2}{r^2} e^{-2m_s r}$	$c_n \frac{m_s^2}{r^2} e^{-2m_s r}$	$-\frac{2}{3} c_n \frac{m_s^2}{r^2} e^{-2m_s r}$	$c_n \frac{m_s}{r^3} e^{-2m_s r}$
proton	$\frac{1}{2} c_p \frac{1}{r^4}$	$-c_p \frac{1}{r^4}$	$\frac{1}{6} c_p \frac{1}{r^4}$	$-\frac{1}{2} c_p \frac{1}{r^4}$

TABLE I: Behavior of neutron and proton EMT distributions at asymptotic distances $m_s r \gg 1$. The neutron asymptotics are determined by the scalar field with $c_n = b_n^2 e^{2m_s R_n} / (4\pi g_s)^2$ and the proton ones by the Coulomb field with $c_p = \frac{\alpha}{4\pi} \hbar c$.

VI. EMT FORM FACTORS AND THE D -TERM

The proton $D(t)$ was computed in [40] from $p(r)$ and $s(r)$ in (5) which yields the same result. Here we use the same technique for the neutron case. The form factor $A(t)$ was not discussed in [40]. We compute it using Eq. (3) where, strictly speaking, the knowledge of the form factor $B(t) = A(t) - 2J(t)$ is needed with $J(t)$ the angular momentum form factor satisfying $J(0) = \frac{1}{2}$ for a spin- $\frac{1}{2}$ particle. $J(t)$ can be determined from the $T_{0k}(\vec{r})$ components of the EMT which vanish for the static (non-rotating) proton and neutron solutions in the classical model. In principle, one could use standard projection techniques [58] to assign definite spin quantum numbers to our “mean field” solutions to obtain non-zero results for $T_{0k}(\vec{r})$. We will refrain from this step and content ourselves with a very good approximation which consists in neglecting $B(t)$ in Eq. (3). This step is justified in the large N_c limit $|t| \sim N_c^0 \ll M^2 \sim N_c^2$ where the form factors $A(t)$, $B(t)$, $J(t)$ behave like N_c^0 while $D(t) \sim N_c^2$ [9] which allows one to neglect $|B(t)| \ll |D(t)|$ in Eq. (3). This result is strongly supported by lattice QCD results where $|B(t)| \ll |D(t)|$ is found [35]. The form factors $A(t)$ and $D(t)$ of proton and neutron obtained in this way in the classical model are shown in Fig. 3.

The form factor $A(t)$ must satisfy the constraint $A(0) = 1$, and the model results comply with this requirement. Numerically, the proton and neutron $A(t)$ form factors can hardly be distinguished on the scale of Fig. 3a. In Fig. 3b we show $D(t)$ of the neutron and proton using the same scale as in Fig. 3a to demonstrate that also in the case of $D(t)$ the proton and neutron results can hardly be distinguished on the scale of the figure for $(-t) \gtrsim 0.1 \text{ GeV}^2$. The difference between neutron and proton $D(t)$ becomes apparent only in the region $(-t) \ll 0.1 \text{ GeV}^2$ displayed in Fig. 3c with a logarithmic scale for the $(-t)$ -axis for better visibility. As can be seen in Fig. 3c, the neutron $D(t)$ form factor remains negative and approaches a well-defined value for $t \rightarrow 0$. The proton $D(t)$ form factor starts to deviate from the neutron case more and more strongly with decreasing $(-t)$ and changes sign at $t \simeq -3 \times 10^{-4} \text{ GeV}^2$. Eventually for $(-t) \lesssim 10^{-6} \text{ GeV}^2$ the proton $D(t)$ diverges according to the QED prediction [41]

$$D(t) = \alpha \frac{\pi M}{4\sqrt{-t}} + \dots, \quad (19)$$

where the dots indicate subleading terms as $t \rightarrow 0$. In [40] the proton $D(t)$ form factor was studied down to $(-t) = 10^{-8} \text{ GeV}^2$ and the classical proton model was demonstrated to reproduce the QED prediction (19).

In the model, the reason for the divergence of the proton $D(t)$ in Eq. (19) is due to the large- r behavior of the Coulomb field. The neutron EMT distributions decay exponentially at large r , see Table I, and the integrals defining the D -term in Eq. (8) converge such that one obtains a well-defined and unambiguous result for D_{neut} . In the proton case, however, the Coulomb field determines the asymptotics, see Table I, and the corresponding integrals diverge. In Ref. [40] it was proposed to introduce a “regularized” proton D -term $D_{\text{prot,reg}}$. In the remainder of this section, we will review how this regularization works and, based on the neutron results, show that it is reasonable. In Sec. VIII we will provide an argument why a regularized proton D -term makes sense also from a practical point of view.

The starting point to define a regularized $D_{\text{prot,reg}}$ in [40] was the observation that, in a theory where the integrals converge, one may use D_{press} or D_{shear} in Eq. (8), or any linear combination $D(\zeta) = \zeta D_{\text{press}} + (1 - \zeta) D_{\text{shear}}$ to obtain the same result for any ζ . In the proton case, $D(\zeta)$ diverges for all ζ except for one special value $\zeta_{\text{reg}} = \frac{8}{3}$ when

$$D_{\text{prot,reg}} = D(\zeta)|_{\zeta=\frac{8}{3}} = M \int d^3r r^2 \left[\frac{8}{3} p(r) + \frac{4}{9} s(r) \right] \quad (20)$$

is finite because the square bracket under the integral corresponds to $\frac{4}{9} [6p(r) + s(r)]$ where the Coulomb tails in Table I cancel out exactly [40].

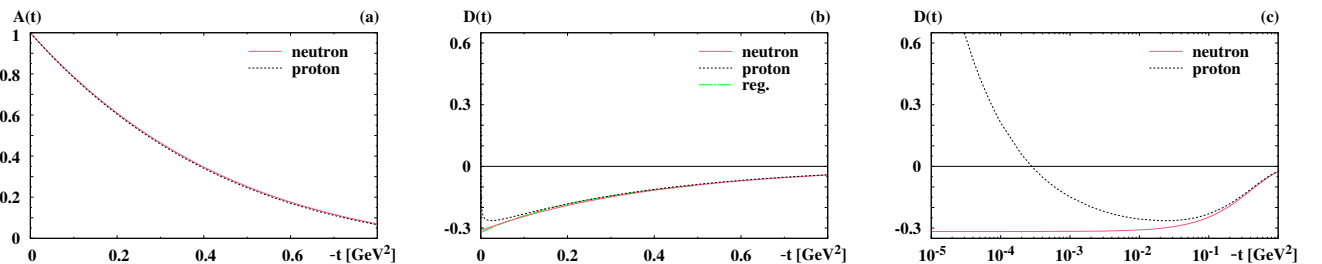


FIG. 3: Form factors $A(t)$ (a) and $D(t)$ (b) of neutron and proton vs. $(-t)$ in the classical model. (c) The same as panel (b) but with logarithmic t -scale to display the region $(-t) \ll 0.1 \text{ GeV}^2$ where neutron and proton $D(t)$ exhibit different properties.

Let us present now an independent regularization method that can be applied to the D -term and other quantities. Let $F(r)$ be an EMT distribution in the proton with the asymptotics in Table I. Consider the integral $I_n = \int d^3r r^n F(r)_{\text{reg}}$ with $n > 1$ which diverges at large r and needs to be regularized as indicated by the subscript. We subtract under the integral of I_n a second term which is identically zero due to Eq. (6a) as follows

$$I_n = \int d^3r \left[r^n F(r) - Z_F r^{n+1} \left\{ \frac{2}{3} s'(r) + \frac{2}{r} s(r) + p'(r) \right\} \right]_{\text{reg}}$$

with the constant Z_F to be defined shortly. In the next step, we carry out an integration by parts in the second term and “neglect” a divergent boundary term at $r \rightarrow \infty$ which we define to be permissible under the regularization prescription. We obtain

$$I_n = \int d^3r r^n \left[F(r) + Z_F \left\{ \frac{2}{3} n s(r) + (n+3) p(r) \right\} \right]_{\text{reg}}$$

At large r the linear combination $\frac{2}{3} n s(r) + (n+3) p(r) = -\frac{1}{2}(n-1) \frac{\alpha}{4\pi} \frac{1}{r^4}$. We therefore define the constant Z_F as

$$Z_F = \lim_{r \rightarrow \infty} \frac{r^4 F(r)}{\frac{1}{2}(n-1) \frac{\alpha}{4\pi}}.$$

With Z_F defined in this way, the integral is finite. We thus define our regularization prescription to be

$$I_n = \int d^3r r^n F(r)_{\text{reg}} = \int d^3r r^n \left[F(r) + Z_F \left\{ \frac{2}{3} n s(r) + (n+3) p(r) \right\} \right] = \text{finite}. \quad (21)$$

This regularization method has the advantage that it can be applied to any EMT property. Applying this method to the D -term where $n = 2$ and $F(r) = p(r)$ with $Z_F = \frac{1}{3}$ or $F(r) = -\frac{4}{15} s(r)$ with $Z_F = \frac{8}{15}$ we obtain

$$D_{\text{prot,reg}} = \begin{cases} M \int d^3r r^2 p(r)_{\text{reg}} = M \int d^3r r^2 \left[p(r) + \frac{1}{3} \left\{ \frac{4}{3} s(r) + 5 p(r) \right\} \right], \\ -\frac{4}{15} M \int d^3r r^2 s(r)_{\text{reg}} = M \int d^3r r^2 \left[-\frac{4}{15} s(r) + \frac{8}{15} \left\{ \frac{4}{3} s(r) + 5 p(r) \right\} \right], \end{cases}$$

which reproduces, in either case, unambiguously the result (20) derived in [40]. Numerically, we obtain

$$D_{\text{neut}} = -0.317 (\hbar c)^2, \quad (22)$$

$$D_{\text{prot,reg}} = -0.322 (\hbar c)^2. \quad (23)$$

Our result for the neutron confirms that the concept of proton D -term regularization proposed in [40] makes physically sense because one expects proton and neutron to have very similar properties if one disregards isospin violating effects and “neglects” electromagnetic effects (with the neglect of electromagnetic effects defined by the above regularization).

Before ending this section, let us briefly explain the dashed dotted line in Fig. 3b which motivated in Ref. [40] the idea to introduce a regularized value $D_{\text{prot,reg}}$. If we refrain from small $(-t)$ where QED effects play a role and large $(-t)$ where the model is not applicable, i.e. if we focus on an intermediate range $0.1 \text{ GeV}^2 \lesssim (-t) \lesssim 0.5 \text{ GeV}^2$, then the proton $D(t)$ can be well approximated by $D(t) \approx D_{\text{prot,reg}} / (1 - t/m_D^2)^n$ with $m_D = 0.985 \text{ GeV}$ and $n = 3$ [40]. In this $(-t)$ -range, this approximation and the numerical proton and neutron results for $D(t)$ can all be hardly distinguished on the scale of Fig. 3b. Thus, $D_{\text{prot,reg}}$ is useful to provide an approximation to the proton $D(t)$ in an intermediate $(-t)$ -range. This is an indication for the practical usefulness of the concept of a regularized proton D -term. We will see a stronger argument in Sec. VIII, after making further use of the new regularization method.

VII. EMT RADII AND NEUTRON SIZE

In Sec. V we saw that the dust distribution in the neutron occupies a smaller volume as compared to the proton with $R_n = 1.04 \text{ fm}$ vs $R_p = 1.05 \text{ fm}$. Within the model, we can use the dust mean square root radii for a somewhat more quantitative comparison of the sizes of neutron and proton which yields

$$\langle r_{\text{dust}}^2 \rangle_n^{1/2} = 0.704 \text{ fm}, \quad \langle r_{\text{dust}}^2 \rangle_p^{1/2} = 0.710 \text{ fm}. \quad (24)$$

In the proton case, the dust radius corresponds to a physical quantity as it defines its charge radius and hence the “proton size”. In the neutron case, there is no such association. The neutron mean square charge radius is with $\langle r_{\text{ch}}^2 \rangle_n = (-0.1155 \pm 0.0017) \text{ fm}^2$ [57] negative and tells us nothing about the “neutron size,” albeit it gives insights about the electric charge distribution in the neutron (whose description is also beyond the present model, see Sec. IV).

In order to meaningfully compare the sizes of proton and neutron, we can make use of the EMT radii in Eq. (9). The latter are well-defined for the neutron but diverge for the proton due to the large- r behavior of the EMT distributions in Table I. In this work, based on the new regularization method in Sec. VI, we are in the position to compute these quantities for the proton and compare to the corresponding neutron results. To regularize the proton EMT radii, we use Eq. (21) with $n = 2$ and respectively $F(r) = \frac{2}{3} s(r) + p(r)$ with $Z_F = -1$ for the mechanical radius and $F(r) = T_{00}(r)$ with $Z_F = 1$ for the mass radius. The neutron and proton results are

$$\langle r_{\text{mech}}^2 \rangle_{\text{neut}}^{1/2} = 0.769 \text{ fm}, \quad \langle r_{\text{mech}}^2 \rangle_{\text{prot,reg}}^{1/2} = 0.797 \text{ fm}, \quad (25)$$

$$\langle r_{\text{mass}}^2 \rangle_{\text{neut}}^{1/2} = 0.755 \text{ fm}, \quad \langle r_{\text{mass}}^2 \rangle_{\text{prot,reg}}^{1/2} = 0.759 \text{ fm}. \quad (26)$$

Several comments are in order. We recall that the dust radius (24) has a physical meaning (in terms of the charge radius) only for the proton, while the EMT radii (25, 26) are in principle both observable providing a path to a meaningful comparison of the proton and neutron sizes. All neutron and proton radii are numerically very similar, see Eqs. (24–26). However, in all cases the neutron is slightly smaller than the proton. Rather than the absolute numbers in Eqs. (24–26), a more robust model prediction is that the mechanical radii of neutron and proton are respectively 8 % and 12 % larger than the proton charge radius. For both particles, the mass radius is (rounded off) about 6 % larger than the proton charge radius.

The fact that the neutron appears systematically smaller than the proton across the various radii (24–26) can be intuitively understood: the repulsive electrostatic forces present in the proton (but absent in the neutron) tend to spread out the matter distribution in the proton. The effect is relatively small because in the model the electromagnetic forces are three orders of magnitude weaker than strong forces. We recall that the strong forces in the model are the relatively weak residual forces. In nature, the QCD color forces are far stronger such that experimentally one should expect even smaller differences between the EMT radii of proton and neutron.

Noteworthy is that the proton radii in Eqs. (25) and (26) are the results of a regularization which corresponds to subtracting off infinities. It is a remarkable and non-trivial result that our regularization preserves the expected physical feature that the proton is larger (and only slightly larger) than the neutron.

VIII. SIMULATING THE PHYSICAL SITUATION FOR PROTON AND NEUTRON

It is an interesting question whether the divergence for $t \rightarrow 0$ of the $D(t)$ of proton can be observed experimentally. The model can be used to shed light on this question but for that one needs first to make the model description more realistic. For that we will address two aspects. (i) In the model the proton charge radius is about 15 % smaller than the experimental value. (ii) The neutron and regularized proton D -terms are about an order of magnitude smaller than, e.g., the D -terms in the more realistic chiral quark soliton model [15] or in lattice QCD [35].

In order to address these two aspects we introduce two free model parameters λ_m and λ_g which simultaneously rescale respectively the masses m_i and coupling constants g_i of the scalar and vector mesons ($i = S, V$) as follows

$$m_i \rightarrow m'_i = \lambda_m m_i, \quad g_i \rightarrow g'_i = \lambda_g g_i. \quad (27)$$

The neutron stress tensor properties scale homogeneously with λ_m and λ_g (in a specific way depending on the property). In the the proton case, the stress tensor properties scale homogeneously with λ_m (because all the relevant dimensionful parameters are rescaled including the photon mass, $m'_\gamma = \lambda_m m_\gamma$, which happens to be zero) but not with λ_g (because in Eq. (27) we do not rescale simultaneously the electromagnetic coupling constant and keep it fixed). Due to the smallness of the electromagnetic coupling constant there is, however, an approximate scaling with λ_g .²

² The energy density has no definite scaling behavior because the model parameter m_{dust} is adjusted to reproduce the proton mass according to footnote 1 as we vary the λ_i . As a consequence of that, the energy density can turn negative in the vicinity of $r = 0$ for $\lambda_g \geq 2.1$ when $\lambda_m = 0.85$. This may be considered a “finite-size renormalization artifact” in an interacting theory as coupling constants are varied. In practice, renormalization effects do not always preserve all physical properties, like positivity of energy density in this case. As m_{dust} enters only in combination with $\rho(r)$ (normalized to unity) in $T_{00}(r)$, it is just an additive constant in the nucleon mass and does not affect mechanical stability and properties related to the stress tensor.

In this way, in the model the nucleon properties become functions of λ_m and λ_g . As can be seen from the Yukawa tails of the meson fields proportional to $\exp(-m_i r)$, Eqs. (11c, 11d, 15b, 15c), one can think of the change $m_i \rightarrow m'_i$ in Eq. (27) as implying a redefinition of the unit of length. As a consequence, for instance the mean square square root dust radius (which corresponds to the proton charge radius scales) depends on λ_m as

$$\langle r_{\text{dust}}^2(\lambda_m, \lambda_g) \rangle^{1/2} = \lambda_m^{-1} \langle r_{\text{dust}}^2 \rangle^{1/2}. \quad (28)$$

Here and in the following, quantities written without explicit dependence on the λ_i refer to unscaled model results. For instance, in Eq. (28) $\langle r_{\text{dust}}^2 \rangle = \langle r_{\text{dust}}^2(\lambda_m, \lambda_g) \rangle|_{\lambda_m=\lambda_g=1}$.

Setting $\lambda_m = 0.85$ yields a proton charge radius of 0.83 fm in agreement with the experimental result inferred from elastic electron-proton scattering experiments $(0.831 \pm 0.007_{\text{stat}} \pm 0.012_{\text{syst}})$ fm [59]. For this value of λ_m , the electromagnetic proton-neutron mass difference which scales as $(M_{\text{prot}} - M_{\text{neut}})(\lambda_m, \lambda_g)_{\text{e.m.}} = \lambda_m (M_{\text{prot}} - M_{\text{neut}})_{\text{e.m.}}$, is reduced by 15 % which is within the theoretical uncertainties of the lattice result quoted in Eq. (18). We conclude that a rescaling with $\lambda_m = 0.85$ yields a realistic description of the electromagnetic properties. Let us recall that the proton mass is always exactly described according to the parameter fixing adopted in this work, see footnote 1.

A rescaling with $\lambda_g > 1$ increases the strength of the strong model forces which for $\lambda_g = 1$ correspond to residual nuclear forces. To obtain a realistic result for the D -term, the residual nuclear forces need to be scaled up to more adequately simulate the QCD forces. The pressure (similarly the shear force) and the $D(t)$ form factor behave as

$$p(r, \lambda_m, \lambda_g) = \lambda_m^4 \lambda_g^2 p(r \lambda_m^{-1})_{\text{strong}} + \lambda_m^4 p(r \lambda_m^{-1})_{\text{em}}, \quad (29)$$

$$D(t, \lambda_m, \lambda_g) = \lambda_m^{-1} \lambda_g^2 D(t \lambda_m^2)_{\text{strong}} + \lambda_m^{-1} D(t \lambda_m^2)_{\text{em}}. \quad (30)$$

To determine the value of λ_g needed to scale up the strong model forces to obtain a D -term as large as determined in lattice QCD we use as guideline the results from [35] obtained from gauge field configurations generated on a $L^3 \times T = (48a)^3 \times (96a)$ lattice [60] based on Lüscher-Weisz gauge action [61] with $N_f = 2 + 1$ flavors of clover-improved Wilson fermions [62], lattice spacing $a \approx 0.091$ fm, and nearly physical pion masses $m_\pi \approx 170$ MeV [63].

In the lattice study [35] results for the total (quark + gluon) nucleon $D(t)$ form factor were presented which is renormalization scale independent allowing one to carry out a direct comparison to a low-energy effective theory such as our model. In the lattice calculation [35] isospin breaking and electromagnetic effects were not considered. This makes the proton as studied in [35] electrically neutral and mass-degenerate with the neutron. The D -term appears in the decomposition of EMT matrix elements with two powers of Δ^μ in Eq. (1) and cannot be computed on the lattice at zero momentum transfer. The smallest available value in [35] was $(-t) = 0.067 \text{ GeV}^2$. The extrapolation to $t = 0$ can be obtained by different methods with similar results. For definiteness, we use here the dipole fit result which has a somewhat larger uncertainty and hence provides a more conservative estimate for the total nucleon D -term [35]

$$D_{\text{lattice}} = -(3.87 \pm 0.97). \quad (31)$$

Recall that this corresponds to an “uncharged proton” or neutron in the absence of isospin violating effects. In the model this value is reproduced well for $(\lambda_m = 0.85 \text{ and } \lambda_g = (3.2 \pm 0.4))$ which yields respectively

$$D_{\text{neut}} = -(3.88 \pm 0.96), \quad (32)$$

$$D_{\text{prot,reg}} = -(3.89 \pm 0.96). \quad (33)$$

Remarkably, the neutron and regularized proton model results agree within 1‰ accuracy. With λ_m and λ_g fixed in the above-explained way, we obtain the results for $D(t)$ shown in Fig. 4.

Fig. 4a shows that the model results for proton and neutron practically overlap. Although we adjusted the parameter λ_g to reproduce only one single value of $D(t)$ — namely at $t = 0$, i.e. the D -term — we nevertheless observe an excellent agreement with the lattice data [35] over an extended t -range in Fig. 4a. The χ^2 per degree of freedom, $\chi_{d.o.f.}^2$, of the model description of lattice QCD data is $\chi_{d.o.f.}^2 = 1.05$ in the region $(-t) < 0.8 \text{ GeV}^2$. Beyond that we observe a tendency of the model to undershoot the lattice data. We find worse $\chi_{d.o.f.}^2 = 1.27$ for $(-t) < 0.9 \text{ GeV}^2$, and $\chi_{d.o.f.}^2 = 1.65$ for $(-t) < 1 \text{ GeV}^2$, although in view of the simplicity of the model, even the last value is acceptable.

Notice that we adjusted λ_g to describe $D(t)$ at $t = 0$ and made no effort to optimize the χ^2 over a range of t because mean field approaches to form factor computations are expected to become sensitive to relativistic recoil with increasing $(-t)$ with a range of applicability up to $(-t) \approx 1 \text{ GeV}^2$ [51–53]. The description of asymptotically large $(-t)$ is in the regime of perturbative QCD [64, 65] and certainly beyond the scope of effective low energy models. For the following, we conclude that the model gives a very good description of the lattice data on $D(t)$ [35] up to $(-t) \lesssim 1 \text{ GeV}^2$. It is a remarkable and nontrivial outcome that by fixing 1 parameter, λ_g , the model is able to describe $\mathcal{O}(20)$ lattice data points in Fig. 4a (after fixing λ_m by means of the proton charge radius).

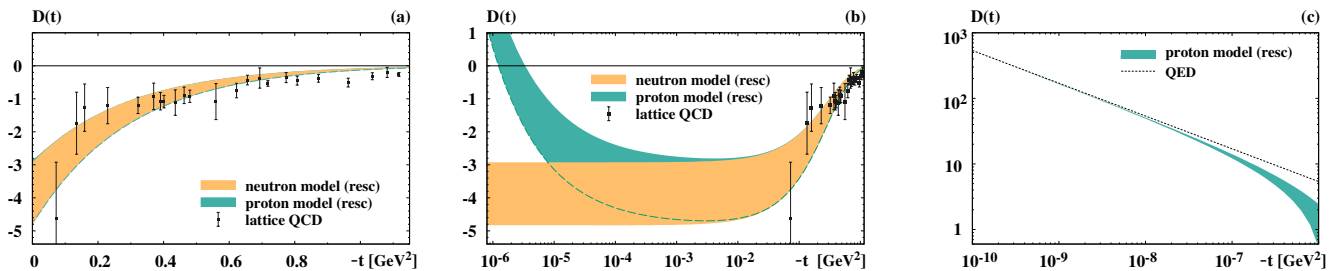


FIG. 4: (a) $D(t)$ of neutron and proton in the model with strong interaction parameters rescaled according to Eq. (27) by $\lambda_m = 0.85$ which yields the correct proton charge radius and $\lambda_g = 3.2 \pm 0.4$ which yields the displayed uncertainty band and a good description of the lattice data from Ref. [35] at $(-t) \lesssim 1 \text{ GeV}^2$ that are shown in the figure for comparison. (b) The same as panel (a) but on a logarithmic $(-t)$ -scale illustrating that the difference between $D(t)$ of neutron and proton becomes noticeable only for $(-t) \lesssim 10^{-4} \text{ GeV}^2$. (c) $D(t)$ of proton $(-t) \lesssim 10^{-6} \text{ GeV}^2$ in comparison to the QED prediction.

Fig. 4b shows the same result as Fig. 4a but with a logarithmic scale for the $(-t)$ -axis to illustrate when one may expect to start seeing deviations. Until $(-t) \approx 10^{-4} \text{ GeV}^2$ there is no appreciable difference between the two curves. In other words, until then the proton and neutron form factors $D(t)$ may be expected to look basically the same. A noticeable difference between the $D(t)$ of these two baryons becomes clearly visible only below $(-t) \approx 10^{-5} \text{ GeV}^2$. At still smaller $(-t)$, somewhere in the range $10^{-6} \text{ GeV}^2 < (-t) < 10^{-5} \text{ GeV}^2$ depending on the parameter λ_g , the proton $D(t)$ changes sign and becomes positive.

Fig. 4c shows the proton $D(t)$ in the region $(-t) \leq 10^{-6} \text{ GeV}^2$ where it is positive. The uncertainty band due to $\lambda_g = (3.2 \pm 0.4)$ shrinks visibly as we enter the regime of small $(-t)$ dominated by QED effects. The proton result starts to approach the QED result which is universal for all charged particles, see Eq. (19), for $(-t) \lesssim 10^{-7} \text{ GeV}^2$. On the scale of the double-logarithmic plot in Fig. 4c, the model result for the proton $D(t)$ and the QED result are practically indistinguishable in the region of $10^{-10} \text{ GeV}^2 \leq (-t) \lesssim 10^{-8} \text{ GeV}^2$. At still smaller $(-t)$, our computational method becomes numerically unstable. However, the asymptotic QED result in Eq. (19) can be derived analytically.

For that we use $s(r) = c_p \frac{1}{r^4} + \dots$ for the shear force at $r \gg R_p$ from Table I where $c_p = \frac{\alpha}{4\pi}$ and the parenthesis indicates exponentially decaying terms. With this result, we determine $\tilde{D}(r)$ from Eq. (5) which yields at $r \gg R_p$

$$\tilde{D}(r) = \frac{c_p M}{2r^2} + \dots \quad (34)$$

where the dots indicate exponentially suppressed terms. Now we can invert the Fourier transform in Eq. (5) by separating $\tilde{D}(r)$ in two contributions: one due to strong fields at all r plus the electromagnetic part at $r < R_p$, and the other one due to the electromagnetic part in Eq. (34) at $r > R_p$. The former yields after the Fourier transform a finite contribution at $t = 0$. The latter yields after integrating out the angular variables in spherical coordinates

$$D(t) = \int d^3r e^{i\vec{\Delta} \cdot \vec{r}} \tilde{D}(r) = 2\pi c_p M \int_{R_p}^{\infty} dr \frac{\sin(|\vec{\Delta}|r)}{|\vec{\Delta}|r} + \text{finite} = 2\pi c_p M \frac{1}{\sqrt{-t}} \int_{R_p \sqrt{-t}}^{\infty} dy \frac{\sin y}{y} + \text{finite} \quad (35)$$

where we substituted $y = |\vec{\Delta}|r$ and used $t = -\vec{\Delta}^2$ or $|\vec{\Delta}| = \sqrt{-t}$. In the limit of very small $(-t)$ when $\epsilon = R_p \sqrt{-t} \ll 1$, the integral yields $\frac{\pi}{2} + \epsilon + \mathcal{O}(\epsilon^3)$. The ϵ -terms can be combined with the finite terms. Thus, we obtain

$$D(t) = \frac{\pi^2 c_p M}{\sqrt{-t}} + \text{finite} = \alpha \frac{\pi M}{4\sqrt{-t}} + \text{finite} \quad (36)$$

which agrees with the QED result in Eq. (19).

Thus, the model exactly reproduces the QED prediction in the limit $t \rightarrow 0$ and lattice QCD in the region for $0.06 \text{ GeV}^2 < t \lesssim 1 \text{ GeV}^2$ which gives confidence that it can reasonably interpolate between what we know from QED and lattice QCD about the $D(t)$ form factor of the proton. Based on our model results, we can draw two conclusions. First, the proton and neutron $D(t)$ can be expected to be practically the same down to $(-t) \approx 10^{-4} \text{ GeV}^2$. Second, it does make sense to introduce the notion of a regularized proton D -term to approximate the exact proton $D(t) \approx D_{\text{prot,reg}} / (1 - t/m_D^2)^n$ with some effective parameter n , for instance, $n = 2$ as used in the lattice data fit in Ref. [35] or $n = 3$ as used in [40] or in the first attempt to extract the proton $D(t)$ from data [66].

IX. CONCLUSIONS

The EMT form factor $D(t)$ of neutral hadrons is negative and finite at $t = 0$, while that of charged hadrons changes sign at small values of $(-t)$ and exhibits for $t \rightarrow 0$ a divergence $D(t) \propto 1/\sqrt{-t}$ as first observed for charged pions in chiral perturbation theory [39] and for proton [40] in the model by Białynicki-Birula [46]. The divergence of $D(t)$ is a universal effect for any charged particle due to the masslessness of the photon [41–43]. In this work, we investigated the important question whether this effect can be observed experimentally for the proton, and whether protons and neutrons must be treated differently in phenomenological studies of hard exclusive reactions.

To address this question, we constructed a classical model of the neutron which differs from the original proton model [40, 46] only by making the dust particles, which constitute the matter in that model, electrically neutral. Despite its simplicity, this simple model accurately accounts for the electromagnetic proton-neutron mass difference. For the neutron we obtain a negative and, for all $(-t)$ -values including $t = 0$, finite $D(t)$ form factor which is numerically very close to the regularized proton D -term proposed in Ref. [40] arguing that the QED divergence of $D(t)$ might most likely be out of reach for experimental detection such that the proton $D(t)$ would practically look finite.

To examine this assertion quantitatively it was necessary to alter the original proton model formulation, where the proton charge radius is about 15 % too small (though “not completely out of touch with reality” [46]) and the D -term is about an order of magnitude smaller [40] compared to results from more realistic hadronic models and lattice QCD (because the residual nuclear forces underlying the model are far weaker than the strong forces between quarks). To make the modelling of the strong forces more realistic, we introduced two model parameters: one to bring the model result for the proton charge radius in agreement with experiment, and the other to bring the model result for the D -term in agreement with lattice data [35]. Remarkably, this resulted in a very good description of lattice QCD data on $D(t)$ up to $(-t) \lesssim 1 \text{ GeV}^2$. We have also analytically proven that the model exactly reproduces the QED divergence of $D(t)$ for the proton.

Equipped with this realistic model incorporating all that is currently known about $D(t)$ from QED and QCD from $t \rightarrow 0$ until $(-t) \lesssim 1 \text{ GeV}^2$, we have shown that one would need to go to $(-t)$ below 10^{-4} GeV^2 to observe deviations between the proton and neutron $D(t)$ form factors. In order to verify experimentally the QED prediction for the proton $D(t) = \alpha \pi M / (4\sqrt{-t}) + \dots$ one would need to reach $(-t)$ values of 10^{-8} GeV^2 or smaller. In the very first attempt to extract information related to $D(t)$ from Jefferson Lab data the minimal $(-t)$ value was $(-t)_{\min} = 0.09 \text{ GeV}^2$ [66]. Impact studies for the planned Electron-Ion Collider assume $(-t_{\min}) = 0.03 \text{ GeV}^2$ [67, 68]. Our study therefore leads to the conclusion that in foreseeable future, the experimental observation of QED effects in the proton $D(t)$ will be out of reach. This means that, for all practical purposes in phenomenological studies of hard exclusive reactions, the proton and neutron $D(t)$ will look the same: negative and finite down to the lowest measurable $(-t)$ values in ongoing and planned experiments. This implies that it is a reasonable step to introduce the notion of a “regularized proton D -term” $D_{\text{prot,reg}}$ for Ansätze of the type $D(t) \approx D_{\text{prot,reg}} / (1 - t/m_D^2)^n$ for the proton for $(-t) > 10^{-4} \text{ GeV}^2$ in phenomenological applications and which can be expected to be very similar to the neutron D -term. In fact, in the model D_{neut} and $D_{\text{prot,reg}}$ coincide within 1 % accuracy.

We generalized the method to regularize the proton D -term of Ref. [40] to other EMT properties, and explored it to compute the EMT radii of proton which are divergent (similarly to the D -term) due to the long-range Coulomb field contribution. Comparing the mechanical radius and the mass radius of the proton to those of the neutron (which are finite), we observed that the neutron is systematically slightly smaller than the proton because latter appears slightly swollen compared to the neutron, due to Coulomb repulsion. As a by-product of this study we point out that the EMT radii allow, in contrast to the mean square charge radius, the neutron size. According to the model, proton and neutron will appear as nearly the same size — as one would intuitively expect for these SU(2) partners which are very similar in so many respects, if one refrains from electromagnetic corrections and isospin breaking effects. Based on measurements of the hard exclusive reactions, it will be possible to test this prediction experimentally.

Acknowledgments. The authors are indebted to Phiala Shannahan for sharing the lattice results from Ref. [35]. This work was supported by NSF under the Award No. 2412625, and DOE under the umbrella of the Quark-Gluon Tomography (QGT) Topical Collaboration with Award No. DE-SC0023646.

-
- [1] X. D. Ji, Phys. Rev. Lett. **78**, 610 (1997).
 - [2] I. Y. Kobzarev and L. B. Okun, Zh. Eksp. Teor. Fiz. **43**, 1904 (1962) [Sov. Phys. JETP **16**, 1343 (1963)].
H. Pagels, Phys. Rev. **144**, 1250 (1966).
 - [3] D. Müller, D. Robaschik, B. Geyer, F.-M. Dittes and J. Hořejši, Fortsch. Phys. **42**, 101 (1994). X. D. Ji, Phys. Rev. D **55**, 7114 (1997). A. V. Radyushkin, Phys. Lett. B **380**, 417 (1996); Phys. Lett. B **385**, 333 (1996). J. C. Collins, L. Frankfurt

- and M. Strikman, Phys. Rev. D **56**, 2982 (1997).
- [4] X. D. Ji, J. Phys. G **24**, 1181 (1998). A. V. Radyushkin, arXiv:hep-ph/0101225. K. Goeke, M. V. Polyakov, M. Vanderhaeghen, Prog. Part. Nucl. Phys. **47**, 401 (2001). M. Diehl, Phys. Rept. **388** (2003) 41. A. V. Belitsky and A. V. Radyushkin, Phys. Rept. **418**, 1 (2005). S. Boffi and B. Pasquini, Riv. Nuovo Cim. **30**, 387 (2007). M. Guidal, H. Moutarde, M. Vanderhaeghen, Rept. Prog. Phys. **76**, 066202 (2013). K. Kumericki, S. Liuti, H. Moutarde, Eur. Phys. J. A **52** (2016) 157.
 - [5] M. V. Polyakov and C. Weiss, Phys. Rev. D **60**, 114017 (1999).
 - [6] M. V. Polyakov, Phys. Lett. B **555**, 57 (2003).
 - [7] C. Lorcé, H. Moutarde and A. P. Trawiński, Eur. Phys. J. C **79**, 89 (2019).
 - [8] A. Freese and G. A. Miller, Phys. Rev. D **103**, 094023 (2021).
 - [9] M. V. Polyakov and P. Schweitzer, Int. J. Mod. Phys. A **33**, 1830025 (2018).
 - [10] V. D. Burkert, L. Elouadrhiri, F. X. Girod, C. Lorcé, P. Schweitzer, P. E. Shanahan, Rev. Mod. Phys. **95**, 041002 (2023).
 - [11] C. Lorcé and P. Schweitzer, Acta Phys. Polon. B **56**, 3-A17 (2025).
 - [12] X. D. Ji, W. Melnitchouk and X. Song, Phys. Rev. D **56**, 5511 (1997).
 - [13] V. Y. Petrov, P. V. Pobylitsa, M. V. Polyakov, I. Bönig, K. Goeke and C. Weiss, Phys. Rev. D **57**, 4325 (1998).
 - [14] P. Schweitzer, S. Boffi and M. Radici, Phys. Rev. D **66**, 114004 (2002).
 - [15] K. Goeke, J. Grabis, J. Ossmann, M. V. Polyakov, P. Schweitzer, A. Silva and D. Urbano, Phys. Rev. D **75**, 094021 (2007).
 - [16] K. Goeke, J. Grabis, J. Ossmann, P. Schweitzer, A. Silva and D. Urbano, Phys. Rev. C **75**, 055207 (2007).
 - [17] M. Wakamatsu, Phys. Lett. B **648**, 181 (2007).
 - [18] C. Cebulla, K. Goeke, J. Ossmann and P. Schweitzer, Nucl. Phys. A **794**, 87 (2007).
 - [19] J. H. Jung, U. Yakhshiev and H. C. Kim, J. Phys. G **41**, 055107 (2014).
 - [20] H. C. Kim, P. Schweitzer and U. Yakhshiev, Phys. Lett. B **718**, 625 (2012).
 - [21] J. H. Jung, U. Yakhshiev, H. C. Kim and P. Schweitzer, Phys. Rev. D **89**, 114021 (2014).
 - [22] M. Mai and P. Schweitzer, Phys. Rev. D **86**, 076001 (2012); Phys. Rev. D **86**, 096002 (2012).
 - [23] M. Cantara, M. Mai and P. Schweitzer, Nucl. Phys. A **953**, 1 (2016).
 - [24] I. A. Perevalova, M. V. Polyakov and P. Schweitzer, Phys. Rev. D **94** (2016) 054024.
 - [25] I. Gulamov, E. Nugaev, A. Panin and M. Smolyakov, Phys. Rev. D **92**, 045011 (2015). E. Nugaev and A. Shkerin, J. Exp. Theor. Phys. **130**, 301-320 (2020).
 - [26] P. Hägler *et al.* [LHPC and SESAM Collaborations], Phys. Rev. D **68**, 034505 (2003). M. Göckeler *et al.* [QCDSF Collaboration], Phys. Rev. Lett. **92**, 042002 (2004). P. Hägler *et al.* [LHPC Collaboration], Phys. Rev. D **77**, 094502 (2008).
 - [27] P. E. Shanahan and W. Detmold, Phys. Rev. Lett. **122**, 072003 (2019); Phys. Rev. D **99**, 014511 (2019).
 - [28] B. Pasquini, M. V. Polyakov and M. Vanderhaeghen, Phys. Lett. B **739**, 133 (2014).
 - [29] J. Hudson and P. Schweitzer, Phys. Rev. D **96**, 114013 (2017); Phys. Rev. D **97**, 056003 (2018).
 - [30] I. Anikin, Phys. Rev. D **99**, 094026 (2019).
 - [31] M. J. Neubelt, A. Sampino, J. Hudson, K. Tezgin and P. Schweitzer, Phys. Rev. D **101**, 034013 (2020).
 - [32] K. Azizi and U. Özdem, Eur. Phys. J. C **80**, 104 (2020). U. Özdem and K. Azizi, Phys. Rev. D **101**, 114026 (2020).
 - [33] J. Gegelia and M. V. Polyakov, Phys. Lett. B **820**, 136572 (2021).
 - [34] C. Lorcé, P. Schweitzer and K. Tezgin, Phys. Rev. D **106**, 014012 (2022).
 - [35] D. C. Hackett, D. A. Pefkou and P. E. Shanahan, Phys. Rev. Lett. **132** (2024) 251904.
 - [36] X. H. Cao, F. K. Guo, Q. Z. Li, B. W. Wu and D. L. Yao, [arXiv:2507.05375 [hep-ph]].
 - [37] Z. Dehghan and K. Azizi, Phys. Rev. D **112**, 054014 (2025).
 - [38] W. Broniowski and E. Ruiz Arriola, Phys. Rev. D **78**, 094011 (2008); Phys. Lett. B **859**, 139138 (2024); Acta Phys. Polon. B **56**, 3-A18 (2025); Phys. Rev. D **112**, 054028 (2025).
 - [39] B. Kubis and U. G. Meissner, Nucl. Phys. A **671**, 332 (2000) [Erratum-ibid. A **692**, 647 (2001)].
 - [40] M. Varma and P. Schweitzer, Phys. Rev. D **102**, 014047 (2020).
 - [41] J. F. Donoghue, B. R. Holstein, B. Garbrecht and T. Konstandin, Phys. Lett. B **529**, 132 (2002) Erratum: [Phys. Lett. B **612**, 311 (2005)].
 - [42] A. Metz, B. Pasquini and S. Rodini, Phys. Lett. B **820** (2021) 136501.
 - [43] A. Freese, A. Metz, B. Pasquini and S. Rodini, Phys. Lett. B **839** (2023) 137768.
 - [44] A. Y. Loginov and V. V. Gauzshtein, Phys. Rev. D **102**, 025010 (2020).
 - [45] J. Y. Panteleeva, Phys. Rev. D **107**, 055015 (2023).
 - [46] I. Białynicki-Birula, Phys. Lett. A **182**, 346 (1993).
 - [47] G. A. Miller, [arXiv:2507.14388 [hep-ph]].
 - [48] X. Ji and C. Yang, [arXiv:2508.16727 [hep-ph]].
 - [49] A. Freese, Phys. Rev. D **112**, 034037 (2025).
 - [50] E. Witten, Nucl. Phys. B **160**, 57 (1979); Nucl. Phys. B **223**, 433 (1983).
 - [51] E. Braaten, S. M. Tse and C. Willcox, Phys. Rev. Lett. **56**, 2008 (1986).
 - [52] X. D. Ji, Phys. Lett. B **254**, 456-461 (1991).
 - [53] C. V. Christov *et al.* Prog. Part. Nucl. Phys. **37**, 91-191 (1996).
 - [54] B. D. Serot and J. D. Walecka, "The Relativistic Nuclear Many-Body Problem," in Advances in Nuclear Physics Vol. 16, Eds. J. W. Negele and E. Vogt, (Plenum, New York, 1986), page 125.
 - [55] V. Punjabi, C. F. Perdrisat, M. K. Jones, E. J. Brash and C. E. Carlson, Eur. Phys. J. A **51**, 79 (2015).

- [56] S. Borsanyi *et al.* [BMW], Science **347**, 1452-1455 (2015).
- [57] S. Navas *et al.* [Particle Data Group], Phys. Rev. D **110** (2024) 030001.
- [58] R. Rajamaran, “Solitons and Instantons Amsterdam,” (North-Holland, Amsterdam, 1982).
- [59] W. Xiong *et al.* Nature **575** (2019) 147-150.
- [60] R. Edwards, R. Gupta, N. Joó, K. Orginos, D. Richards, F. Winter, and B. Yoon, U.S. 2+1 flavor clover lattice generation program, unpublished (2016).
- [61] M. Lüscher and P. Weisz, Commun. Math. Phys. **97**, 59 (1985) [erratum: Commun. Math. Phys. **98**, 433 (1985)].
- [62] B. Sheikholeslami and R. Wohlert, Nucl. Phys. B **259**, 572 (1985).
- [63] S. Park *et al.* Phys. Rev. D **105**, 054505 (2022).
- [64] X. B. Tong, J. P. Ma and F. Yuan, Phys. Lett. B **823**, 136751 (2021).
- [65] X. B. Tong, J. P. Ma and F. Yuan, JHEP **10**, 046 (2022).
- [66] V. D. Burkert, L. Elouadrhiri, and F. X. Girod, Nature **557**, 396 (2018).
- [67] E. C. Aschenauer, S. Fazio, K. Kumerički and D. Müller, JHEP **09**, 093 (2013) [arXiv:1304.0077 [hep-ph]].
- [68] R. Abdul Khalek *et al.* Nucl. Phys. A **1026**, 122447 (2022).